



**Calhoun: The NPS Institutional Archive**  
**DSpace Repository**

---

NPS Scholarship

Publications

---

2000

## Dynamic Stall Alleviation using a Deformable Leading Edge Concept - A Numerical Study

Sahin, Mehmet; Sankar, Lakshmi N.; Chandrasekhara, M.S.; Tung, Chee

American Institute of Aeronautics and Astronautics (AIAA)

---

Mehmet Sahin, Lakshmi Sankar, M. Chandrasekhara, and Chee Tung. "Dynamic stall alleviation using a deformable leading edge concept - A numerical study", 38th Aerospace Sciences Meeting and Exhibit, Aerospace Sciences Meetings, ()  
<https://hdl.handle.net/10945/50219>

---

This publication is a work of the U.S. Government as defined in Title 17, United States Code, Section 101. Copyright protection is not available for this work in the United States.

*Downloaded from NPS Archive: Calhoun*



Calhoun is the Naval Postgraduate School's public access digital repository for research materials and institutional publications created by the NPS community. Calhoun is named for Professor of Mathematics Guy K. Calhoun, NPS's first appointed -- and published -- scholarly author.

**Dudley Knox Library / Naval Postgraduate School**  
**411 Dyer Road / 1 University Circle**  
**Monterey, California USA 93943**

<http://www.nps.edu/library>

**AIAA 2000-0520**

**Dynamic Stall Alleviation using a  
Deformable Leading Edge Concept - A  
Numerical Study**

Mehmet Sahin, Lakshmi N. Sankar  
School of Aerospace Engineering  
Georgia Institute of Technology, Atlanta, GA 30332-0150

M. S. Chandrasekhara  
Department of Aeronautics and Astronautics  
Naval Postgraduate School, Monterey, CA 93943

Chee Tung  
Army/NASA Rotorcraft Division  
Aerodynamics Directorate (AMRDEC), AMCOM  
NASA Ames Research Center, Moffett field, CA 94035-1000

# Dynamic Stall Alleviation using a Deformable Leading Edge Concept - A Numerical Study

Mehmet Sahin<sup>\*</sup>, Lakshmi N. Sankar<sup>\*\*</sup>  
School of Aerospace Engineering  
Georgia Institute of Technology, Atlanta, GA 30332-0150

M. S. Chandrasekhara<sup>§</sup>  
Department of Aeronautics and Astronautics  
Naval Postgraduate School, Monterey, CA 93943

Chee Tung<sup>†</sup>  
Army/NASA Rotorcraft Division  
Aerodynamics Directorate (AMRDEC), AMCOM  
NASA Ames Research Center, Moffett field, CA 94035-1000

## **ABSTRACT**

Dynamic stall calculations were carried out for an airfoil with a deformed leading edge shape at a freestream Mach number of 0.3. The surface deformations were done about a baseline NACA 0012 airfoil, effectively increasing the airfoil leading edge radius and thickness at high angles of attack. It was found that the DDLE airfoil had a slightly dynamic stall behavior compared to the baseline NACA 0012 airfoil. In particular, the lift, drag and pitching moment hysteresis loops were milder for the DDLE airfoil compared to the baseline airfoil. It was also found that a static shape that corresponds to the thickest deformed shape performed just as well as the DDLE shape, indicating that the shape itself, and not its time rate of change, was the reason for the improved performance. At higher Mach numbers around 0.4, the DDLE shape exhibited a strong dynamic stall triggered by a shock induced separation, offsetting any benefit from the change in the shape of the airfoil. Additional work is needed on the development of DDLE shapes that will perform well at higher speeds.

## **INTRODUCTION**

Rotary wing aircraft often experience a dynamic stall phenomenon over the retreating blade. Three types of stall - light stall, moderate stall, and strong dynamic stall - have been observed in literature<sup>[1]</sup>. The strong dynamic stall phenomenon involves three phases. The lift initially increases as the airfoil pitches up, and continues to increase

well past the static stall value,  $C_{l,max}$ . Towards the end of the upstroke, a vortex begins to form near the leading edge and grows in strength. Towards the beginning of the downstroke, or shortly thereafter, this vortex is shed from the upper surface, creating a rapid loss in the bound circulation and lift. As this vortex rolls downstream over the upper surface, it causes large reductions in local pressure, and high nose down pitching moments. As the airfoil pitches down, one or more weaker vortices are shed from the upper surface, creating additional fluctuations in lift and pitching moment. The flow eventually reattaches at lower angles of attack.

The pitching moments, along with its large variations are transferred to the vehicle through pitch links, or a flex-beam. These components may fail as a result of the high cycle fatigue that develops. These loads also cause vibrations of the fuselage, passenger discomfort, and structural fatigue. Many electronic components and systems (e.g. chips mounted on boards) may experience random failures if the g- loads are high enough, and frequent enough to unseat them.

Many dynamic stall load-alleviation concepts have been proposed in literature. Carr and McAlister<sup>[2]</sup> proposed a leading edge slat device, which operates much like a slat on a wing and suppresses the leading edge stall. Tuncer and Sankar<sup>[3]</sup> have numerically studied this using a two-dimensional multi-element dynamic stall solver. A limited number of 3-D calculations have also been done by Bangalore and Sankar<sup>[4]</sup> to demonstrate that leading edge slats are effective in alleviating dynamic stall. The major drawback of slats is the high drag penalty associated with their use at off-design conditions. A retraction mechanism similar to that found on aircraft will be heavy and costly. For these reasons, this device has not been pursued by the industries.

Another concept that is gaining wide attention is the "synthetic jet" concept. In this approach, mass-less jets generated by flexible cavity walls are used to alter the

---

<sup>\*</sup> Graduate Research Assistant, Student Member AIAA.

<sup>\*\*</sup> Regents' professor, Associate Fellow AIAA.

<sup>§</sup> Research Professor and Associate Director, Assoc. Fellow AIAA.

<sup>†</sup> Research Scientist, Associate Fellow AIAA.

Copyright © 2000 by the American Institute of Aeronautics and Astronautics Inc. All rights reserved.

boundary layer behavior and prevent stall<sup>[5]</sup>. If the jets are strong enough, they can act as spoilers destroying lift or as vortex flaps increasing lift. The ability of synthetic jets to eliminate undesirable loads and pitching moments has been computationally studied by Hassan at Boeing Mesa.

A third concept for dynamic stall alleviation is the "Dynamically deforming leading Edge Concept" proposed by Chandrasekhara and Carr<sup>[6]</sup>. In this approach, the airfoil shape is gradually changed, and the leading edge radius is increased as the airfoil pitches up. Airfoils with large leading edge radii tend to have mild adverse pressure gradients, because the peak local velocities are lower than that for a conventional airfoil. As the airfoil pitches down, and there is no danger of stall, the airfoil returns to its original shape.

In this work, the dynamically deforming leading edge concept (DDLE) is computationally studied. A two-dimensional compressible Navier-Stokes solver is used. The baseline shape is a NACA 0012 airfoil, which is deformed according to the schedule prescribed in Ref. 6. It is demonstrated that the dynamic stall process is indeed alleviated by the use of the deforming leading edge shape. This is done through a comparison of the surface pressure distributions and load hysteresis loops for the baseline NACA 0012 airfoil and the DDLE airfoil.

## MATHEMATICAL AND NUMERICAL FORMULATION

A two-dimensional compressible Navier-Stokes solver is used in this study. This solver uses a curvilinear body-fitted grid, that will pitch up or down with the airfoil. The scheme is second order or fourth order accurate in space, and is first order accurate in time. A two-layer eddy viscosity model is used to account for the effects of turbulence. Wu and Sankar describe the mathematical formulation behind this analysis, and applications of this solver<sup>[7]</sup>. Three-dimensional versions of this solver that can model oscillating wings<sup>[8]</sup> and rotors also exist<sup>[9]</sup>.

At each time step, the airfoil surface and the surrounding grid are distorted using the schedule provided in Ref. 6. For the given discrete set of airfoil surface points, the Gram-Schmidt orthonormalization process described in Ref. 10 is used to generate a smooth function defining the airfoil geometry. The dynamic grid adaptation used here is similar to the work of Batina<sup>[11]</sup>. The grid around the body is considered to be a system of interconnected springs. This system is constructed by representing a grid line joining two successive grid points by a tension spring. Whenever the airfoil boundary moves, all the grid nodes must be adjusted so that the nodes are force-free.

The value of spring stiffness determines how much a node will move and can be specified in different ways. In this work, the spring stiffness is assumed inversely

proportional to length of distance between two successive grid points and given as

$$k_{m,k} = 1.0 / \left[ (x_{m,k} - x_{i,j})^2 + (y_{m,k} - y_{i,j})^2 \right]^{p/2} \quad (1)$$

Where  $p$  is a parameter used to control the stiffness of the spring (chosen as 5). The grid deformation due to boundary geometry change is solved explicitly by using several Jacobi iterations.

$$\Delta x_{i,j}^{n+1} = \sum k_{m,k} \Delta x_{m,k}^n / \sum k_{m,k} \quad (2.a)$$

$$\Delta y_{i,j}^{n+1} = \sum k_{m,k} \Delta y_{m,k}^n / \sum k_{m,k} \quad (2.b)$$

where the subscripts  $m,k$  indicate the grid points which are connected to point  $i, j$ . The new location of the interior nodes are determined by

$$x_{i,j}^{n+1} = x_{i,j}^n + \Delta x_{i,j}^{n+1} \quad (3.a)$$

$$y_{i,j}^{n+1} = y_{i,j}^n + \Delta y_{i,j}^{n+1} \quad (3.b)$$

Figure 1 shows the leading edge shapes used. Figure 2 shows the amplitude of deformation, as a function of time. The angle of attack of the airfoil is also shown. Figure 3 shows the body-fitted grid in the vicinity of the leading edge at several time levels. Good clustering of the grid, and near-orthogonality are evident.

## RESULTS AND DISCUSSION

Dynamic stall calculations were done for the baseline airfoil, and the DDLE airfoil. The reduced frequency  $k = \omega c / 2V$  is 0.05, where  $\omega$  is the circular frequency,  $c$  is the airfoil chord, and  $V$  is the freestream velocity. The airfoil pitching motion is described by:

$$\alpha = 10^\circ + 10^\circ \cos(\omega t) \quad (4)$$

Four sets of calculations were done: (i) NACA 0012 airfoil at a freestream Mach number  $M=0.3$ , (ii) DDLE airfoil at  $M=0.3$ , with the variation in shape described in Ref. 6. (iii) the DDLE airfoil with a fixed "thickest" shape at  $M=0.3$ , and (iv) DDLE airfoil at  $M=0.4$ . The Reynolds number in all these cases was 1,065,000.

The present calculations assume that the flow is turbulent everywhere. At the Reynolds number of the experiment, there is a large laminar region present, and the transition point moves with the angle of attack. The transition location dramatically affects the onset of separation, and ultimately, the stall. A sophisticated

transition model is required to be developed for pressure gradient flows for use here. In its absence, a one-to-one comparison between the present theory and experiments is not possible at this time. Nevertheless, the qualitative differences between the NACA 0012 and the DDLE airfoil behavior are in accord with what was observed in the experiments.

#### NACA 0012 vs. DDLE Airfoil:

Figure 4 shows the streamlines, and the vorticity contours around the oscillating NACA 0012 and the DDLE airfoils, at selected instances in time. The surface pressure distribution is also shown at these time levels. During the upstroke, up to an angle of attack of 18 degrees or so, the flow field remains attached over both the airfoils. Some increased thickening of the boundary layer is evident on the upper surface as the angle of attack increases.

Around 19.43 degrees during the upstroke, the NACA 0012 airfoil develops a strong leading edge vortex, seen as a "bump" in the surface pressure distribution in figure 4b. The streamlines show considerable amount of separation and recirculation on the upper surface. In contrast, for the DDLE airfoil, even though the entire upper surface boundary layer has separated, the thickness of the separation bubble is smaller. There is also no evidence of a leading edge vortex in the vorticity contours, or the surface pressure distribution.

At the end of the upper stroke, at  $\alpha = 20$  degrees, the streamline plot and the vorticity contours both indicate that leading edge vortex has already been shed for the NACA 0012 airfoil. There is a considerable loss in lift, as evidenced by the collapse of the suction peak. The DDLE airfoil, in contrast, is just beginning the dynamic stall process. It thus appears that the dynamic stall process is delayed by half a degree or so, as a result of the deforming leading edge action.

During the downstroke, as shown by the pressure, vorticity and streamline plots at  $\alpha = 19.66, 15.31$  degrees, the flow over the NACA 0012 airfoil and that over the DDLE airfoil are completely different. A second vortex forms and sheds over the NACA 0012 airfoil. The DDLE airfoil, on the other hand experiences a gradual attachment of the boundary layer, with the separation point migrating from the leading edge to the trailing edge. It thus appears that the DDLE action dramatically improves the airfoil performance during the downstroke. By the time the airfoil reaches an angle of attack of 10 degrees, the flow field has attached and is well behaved for both the airfoils.

Figure 5 shows the load hysteresis loops for the DDLE airfoil and the baseline NACA 0012 airfoil. As expected, for the NACA 0012 airfoil, the lift drops abruptly twice during the downstroke. The pitching moment distribution also shows two large negative peaks, attributable to the large levels of suction that develop near the airfoil trailing edge as the vortex moves over the airfoil. The DDLE airfoil, on the other hand, shows just a single

drop in the lift and a single peak in the pitching moment. These abrupt variations in the lift and pitching moment directly translate into vibratory loads on the fuselage, and contribute to pitch link fatigue. It is clear that the DDLE airfoil is preferred over the NACA 0012 airfoil from these two (vibratory load and fatigue) considerations.

#### DDLE Airfoil with a Fixed Shape:

Given the benefits of the DDLE airfoil, the following question arises. How much of the benefit is attributable to the changes to the shape, and how much is attributable to the surface dynamics, i.e. the rate of change of slope? To answer this question, the DDLE dynamics stall calculations were repeated, with a fixed shape that corresponds to "Shape 8.5" in Ref. 6. This corresponds to the largest leading edge radius, and the bluntest leading edge. It was found that the streamline, vorticity contour and surface pressure variations with angle of attack behavior were identical to the DDLE shape. The integrated loads, as shown in figure 6, were identical for the DDLE shape (where the airfoil shape continually changes) and the fixed 8.5 shape.

Thus it appears that much of the benefits of the DDLE airfoil were attributable to just the increased leading edge radius, and not the rate of change. A passive well-designed shape should be able to experience a milder dynamic stall for the conditions studied, than the NACA 0012 airfoil.

On the other hand, a blunter, thicker passive airfoil shape may have undesirable high-speed characteristics. The blunter leading edge may lead to high locally supersonic velocities and premature formation of shocks on the advancing side. The DDLE shape is thus a compromise between the baseline airfoil that may have good high-speed characteristics, and a thicker, blunter airfoil that has good dynamic stall characteristics.

#### Behavior of the DDLE Airfoil at Higher Mach Numbers:

To determine the behavior of the DDLE airfoil (with a dynamically changing shape) at higher Mach numbers, the previous calculations were repeated at  $M=0.4$ . Form a visualization of the streamline and vorticity contours (not shown here, for brevity), the following phenomena were observed. The flow separated immediately downstream of the shock wave. During the upstroke, around 15 degrees or so, a weak shock formed on the upper surface. The shock induced separation process, and the gradual upstream migration of the turbulent flow separation point, combined to trigger a dynamic stall event during the upstroke. The flow attempted to recover during the downstroke, but a second vortex quickly formed and shed. The lift, drag and pitching moment variations are shown in figure 7. It appears that the DDLE airfoil, with the surface shape variation schedule given in Ref. 6, was not effective in mitigating the dynamic stall process at this higher Mach

number. Additional studies are needed to arrive at DDLE shapes that behave well at higher Mach numbers.

### **CONCLUDING REMARKS**

Dynamic stall calculations have been carried out for a dynamically deforming leading edge airfoil at two Mach numbers – 0.3 and 0.4. At the lower Mach number, it is found that the DDLE airfoil has better dynamic stall characteristics over a conventional NACA 0012 airfoil. This improvement was found attributable to the shape itself, and not the rate at which the shape was changed. At the higher Mach number, the DDLE shape experienced a shock-induced stall during the upstroke, and its dynamic stall characteristics were quite similar to that of the NACA 0012 airfoil at low Mach numbers. Additional studies are needed to develop deforming leading edge shapes that perform satisfactorily at high Mach numbers.

These results are in qualitative agreement with those described in Ref. 6. Since the flow in that study was transitional in nature, the peak suction developed was smaller than found in the present study. Further, both the shape 8-5 airfoil and the adapting airfoil flows were dynamic stall vortex free. A complete modeling of the transition behavior of the flow may enable better agreement between the present theory and experiments.

### **REFERENCES**

1. Carr, L. W., McAlister, K. W. and McCroskey, W. J., "Analysis of the development of Dynamic Stall from oscillating Airfoil Experiments," NASA TN-D-838270, 1977.
2. Carr, L. W. and McAlister, K. W., "The Effects of Leading Edge Slat on the Dynamic Stall of an oscillating Airfoil," AIAA Paper 85-2533, October 1983.
3. Tuncer, I. And Sankar, L. N., "Unsteady Aerodynamic Characteristics of a Dual-Element Airfoil," Journal of Aircraft, Vol. 31, No. 3, May-June 1994.
4. Bangalore, A. and Sankar, L. N., "Numerical Analysis of Aerodynamic Performance of Rotors with Leading Edge Slats," Journal of Computational Mechanics, Vol. 17, pp. 335-342, 1996.
5. Seifert, A., Bachar, T., Koss, D., Shepshelovich, M. and Wagnanski, I., "Oscillatory Blowing - A Tool to delay Boundary Layer Separation," AIAA Journal, Vol. 31, No. 11, November 1993, pp. 2052-2060.
6. Chandrasekhara, M. S. and Carr, L. W., "Unsteady stall Control using Dynamically Deforming Airfoils," AIAA Journal, Vol. 36, No. 10, 1998.
7. Wu, Jiunn-Chi, Huff, D. and Sankar, L.N., "Evaluation of Three Turbulence Models in Static Airloads-and Dynamic Stall Predictions," Journal of Aircraft, Vol. 27, No. 4, April 1990, pp382-384.
8. Sankar, L. N., Malone, J. B. and Schuster, D., "Euler Solutions for Transonic Flow past a Fighter Wing," Journal of Aircraft, Vol. 24, NO. 1, pp. 10-16, 1987.
9. Bangalore, A and Sankar, L. N., "Forward Flight Analysis of Slatted rotors using Navier-Stokes methods," Journal of Aircraft, Vol. 34, No. 1, January-February 1997, pp. 80-86.
10. Chang I-C., Torres F. J. and Tung C., "Geometric Analysis of Wing Sections", NASA-TM-110346, 1995.
11. Batina J.T. "Unsteady Euler Airfoil Solutions Using Unstructured Dynamic Meshes", AIAA Paper 89-0115.

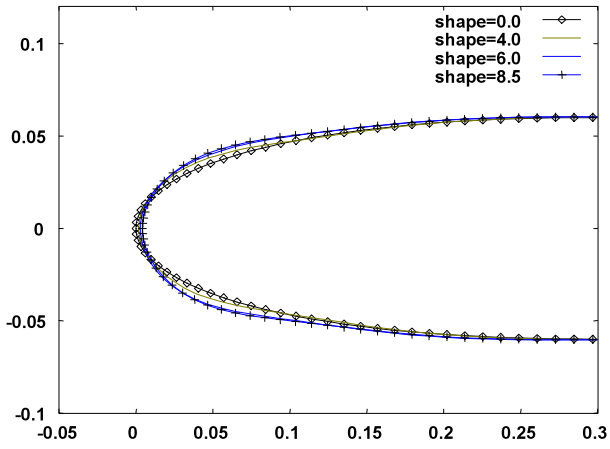


Figure.1.DDLE Airfoil shape profiles

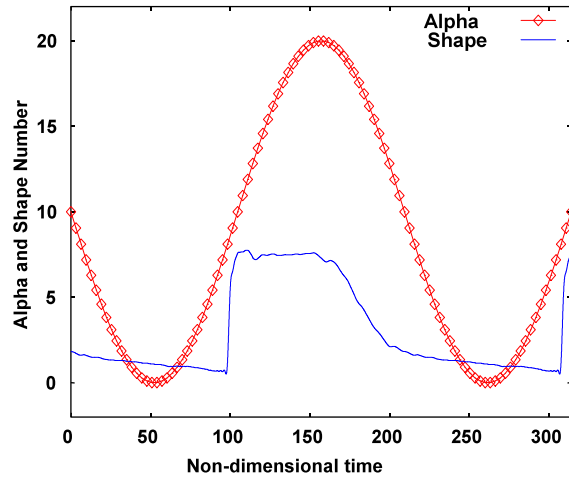


Figure.2. DDLE Shape and Angle of Attach History (V1V05SO-8D5)

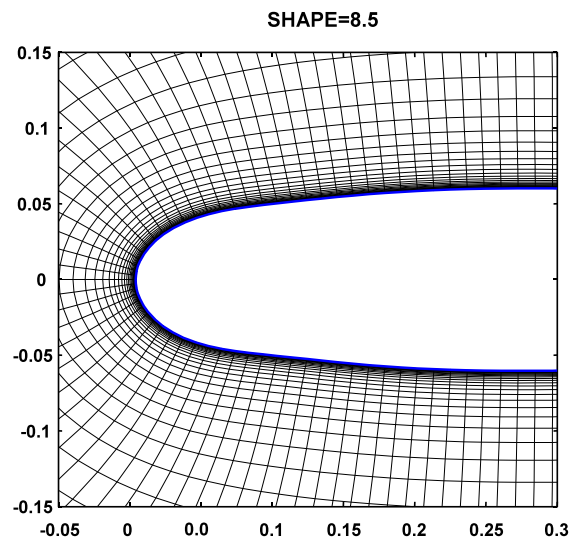
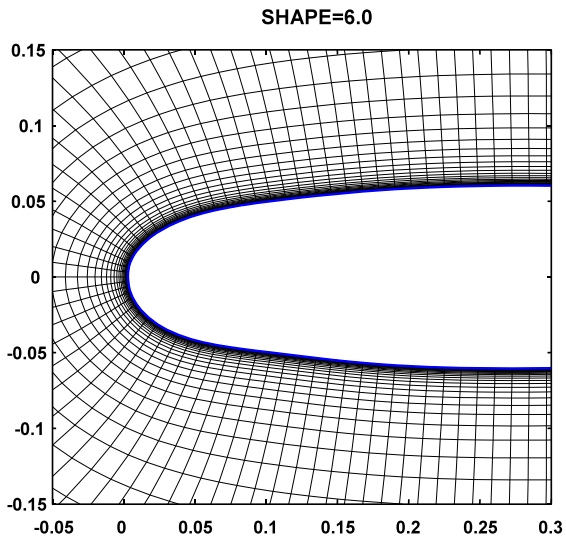
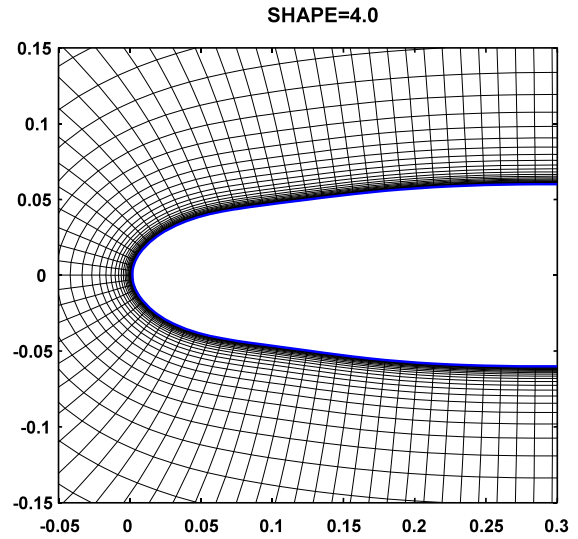
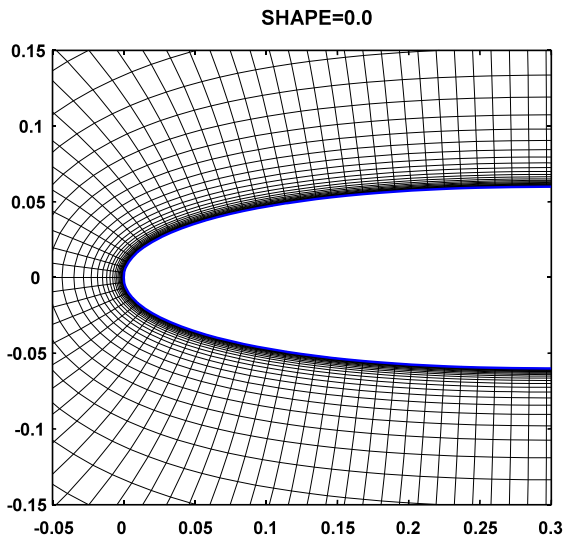
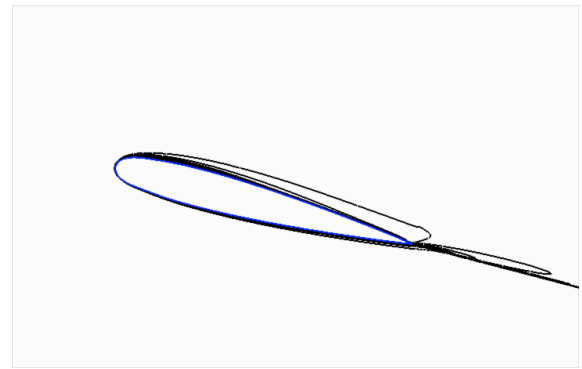
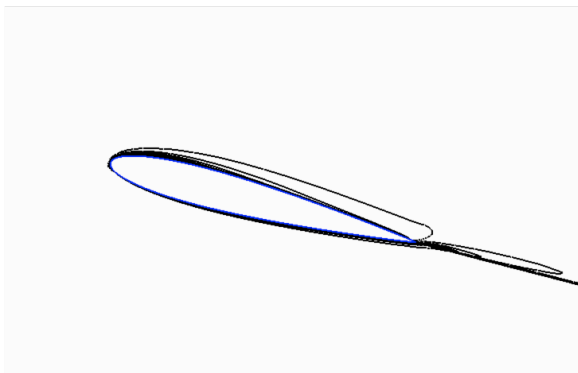
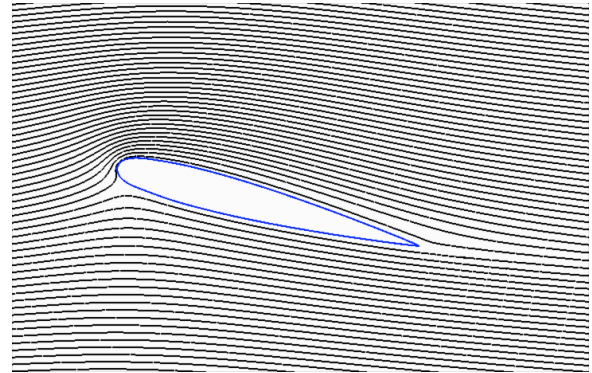
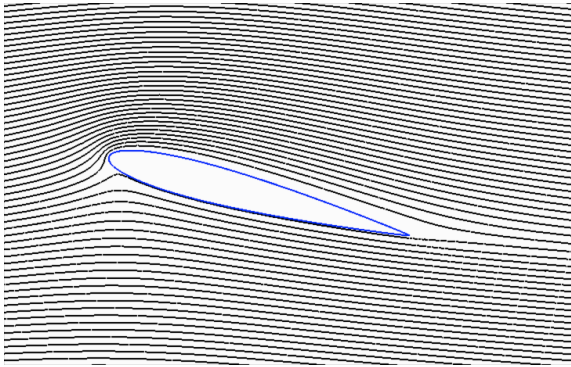
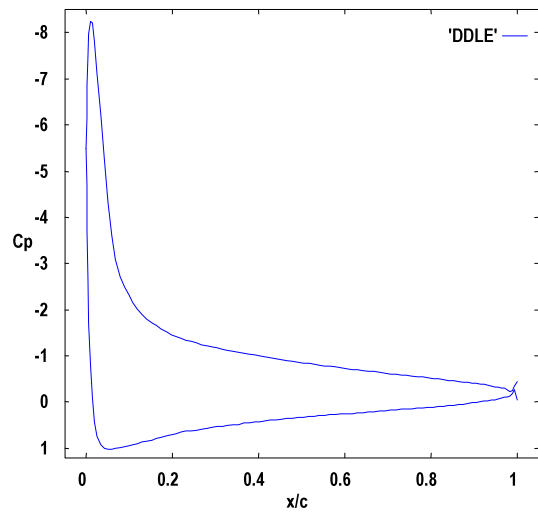
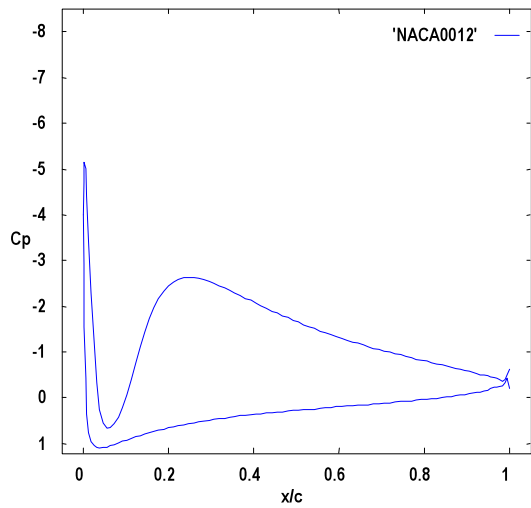
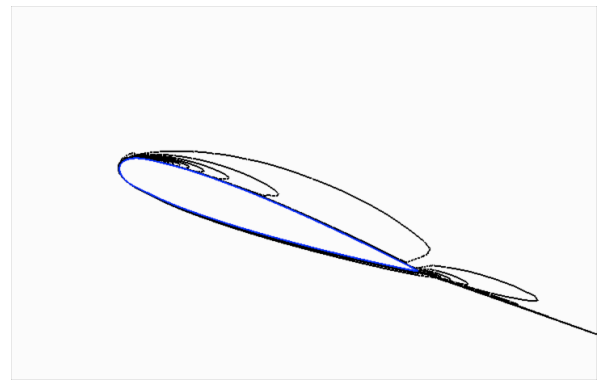
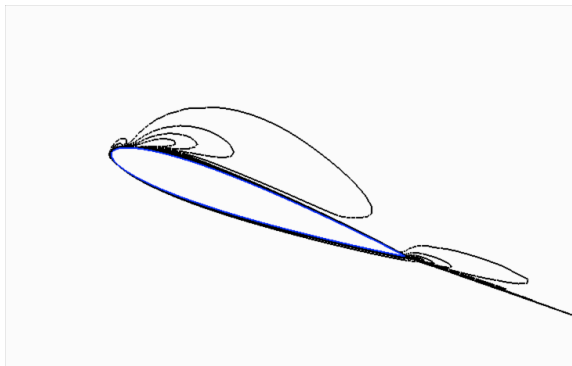
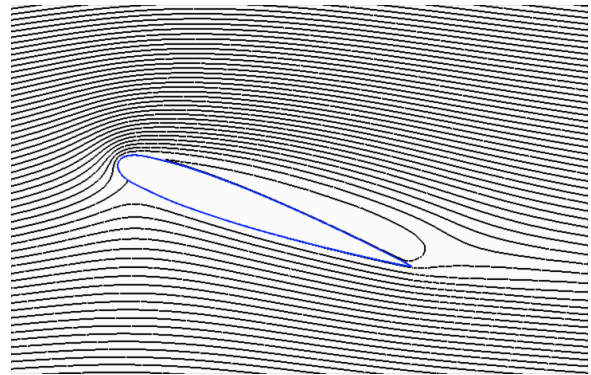
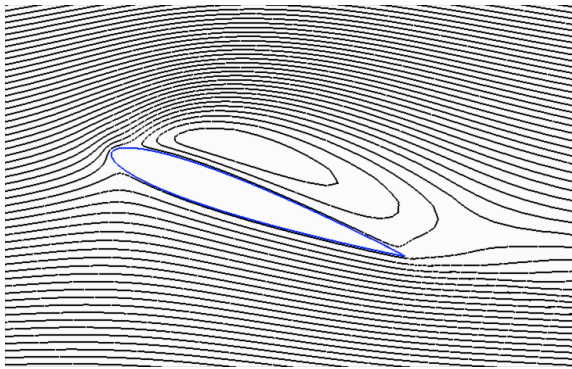


Figure.3. Leading edge grid deformation for DDLE airfoil shape profiles.



**Figure.4.a.1:** Streamlines, vorticity contours and surface pressure coefficient over the NACA0012 airfoil at  $\alpha=14.62^\circ$ .

**Figure.4.a.2:** Streamlines, vorticity contours and surface pressure coefficient over the DDLE airfoil at  $\alpha=14.62^\circ$ .



**Figure.4.b.1:** Streamlines, vorticity contours and surface pressure coefficient over the NACA0012 airfoil at  $\alpha=19.43^\circ$ .

**Figure.4.b.2:** Streamlines, vorticity contours and surface pressure coefficient over the DDLE airfoil at  $\alpha=19.43^\circ$ .

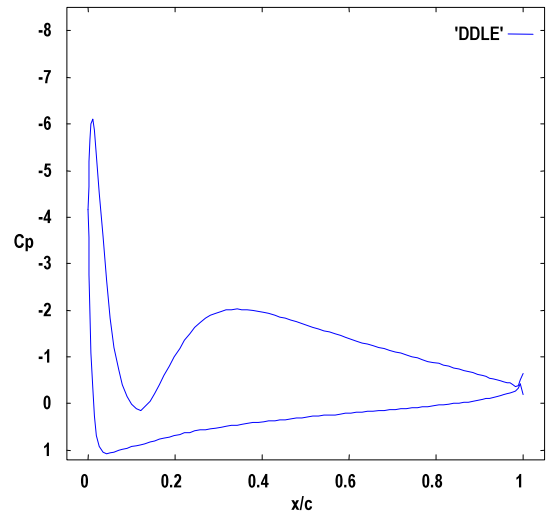
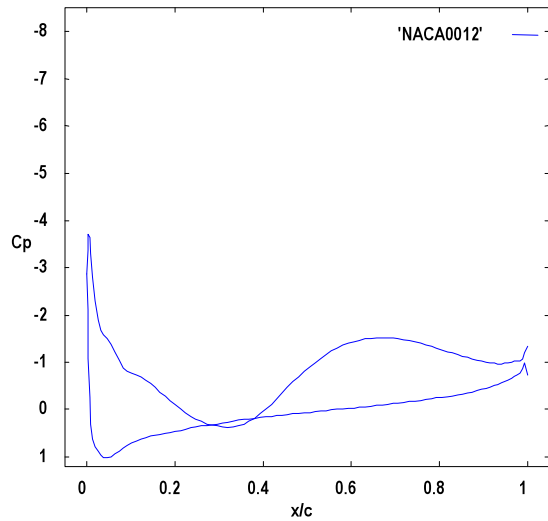
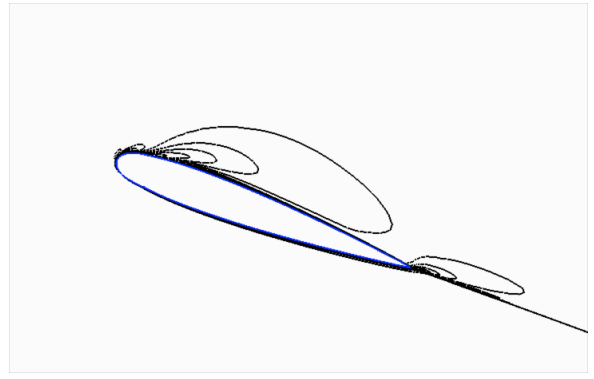
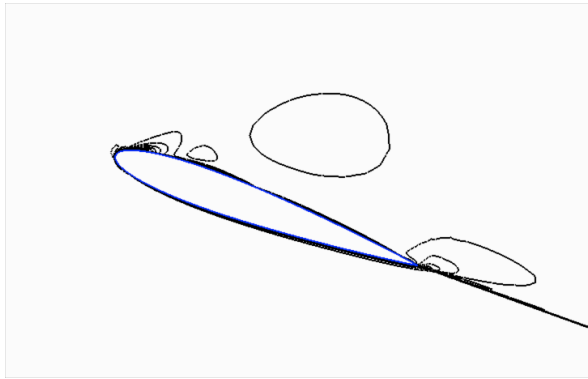
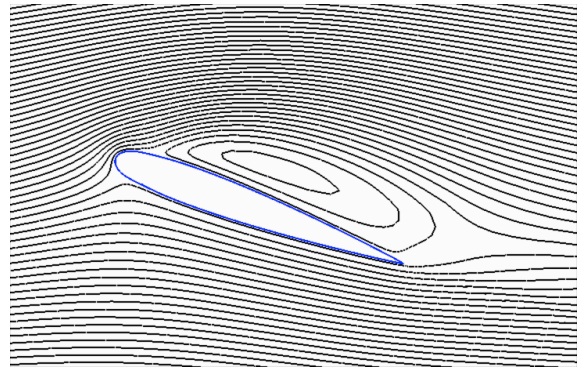
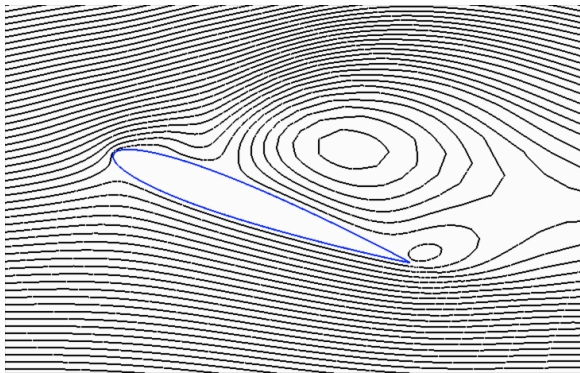


**Figure.4.c.1:** Streamlines, vorticity contours and surface pressure coefficient over the NACA0012 airfoil at  $\alpha = 20.00^\circ$ .

**Figure.4.c.2:** Streamlines, vorticity contours and surface pressure coefficient over the DDLE airfoil at  $\alpha = 20.00^\circ$ .

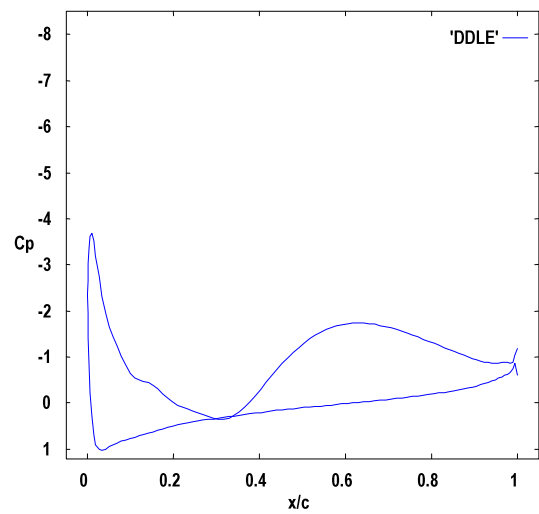
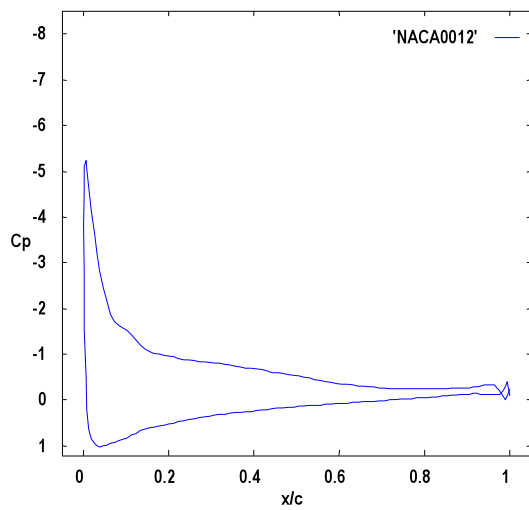
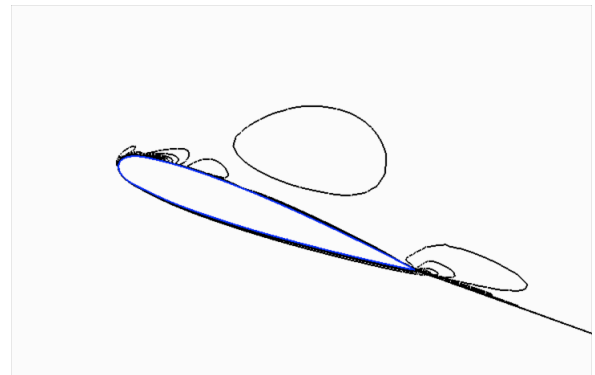
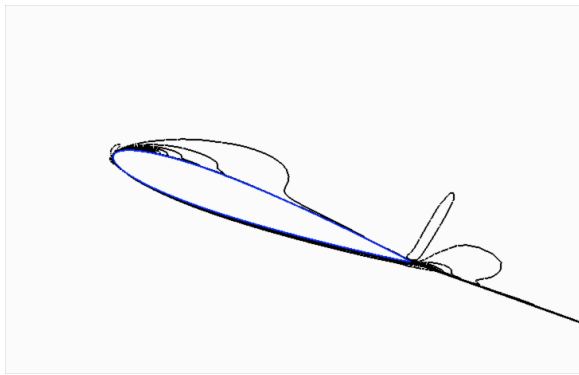
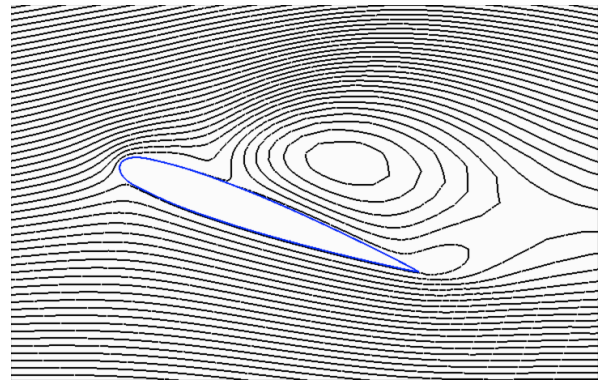
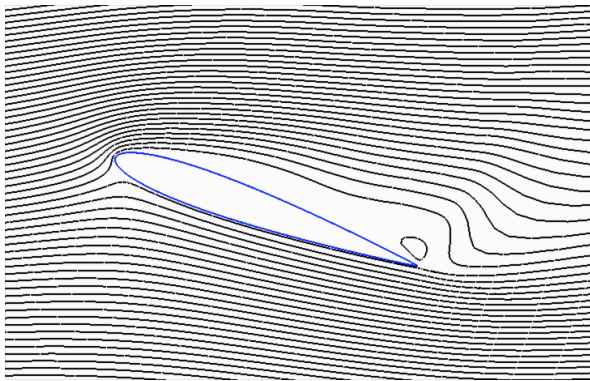


**Figure.4.d.1:** Streamlines, vorticity contours and surface pressure coefficient over the NACA0012 airfoil at  $\alpha=19.66^\circ$ .

**Figure.4.d.2:** Streamlines, vorticity contours and surface pressure coefficient over the DDLE airfoil at  $\alpha=19.66^\circ$ .

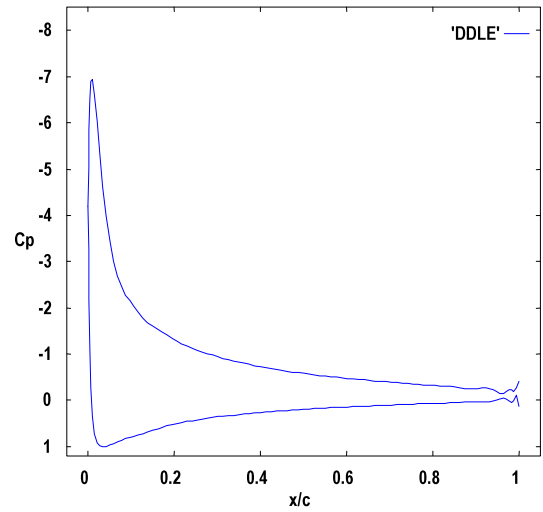
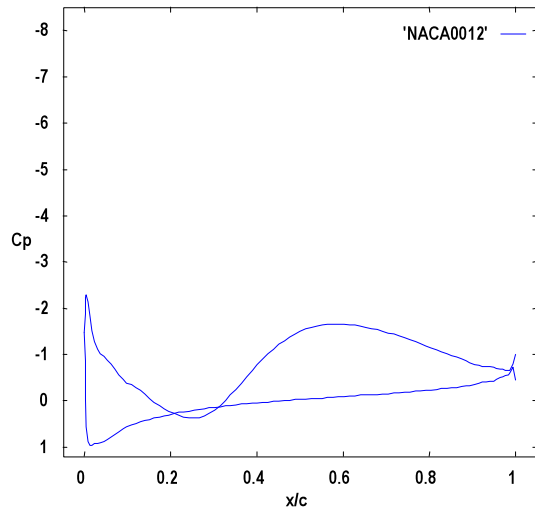
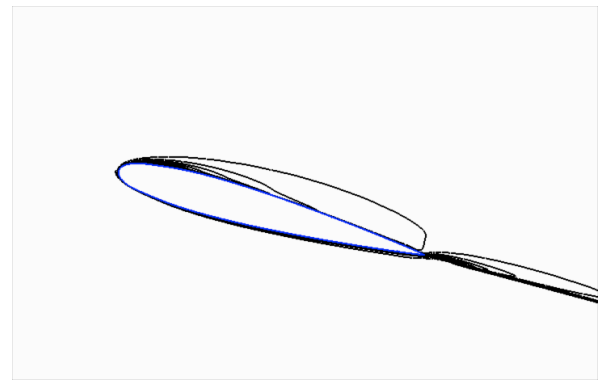
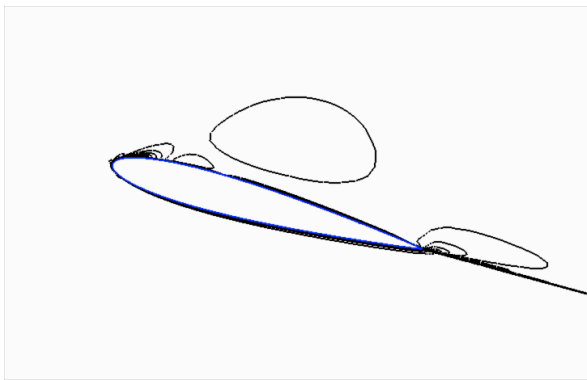
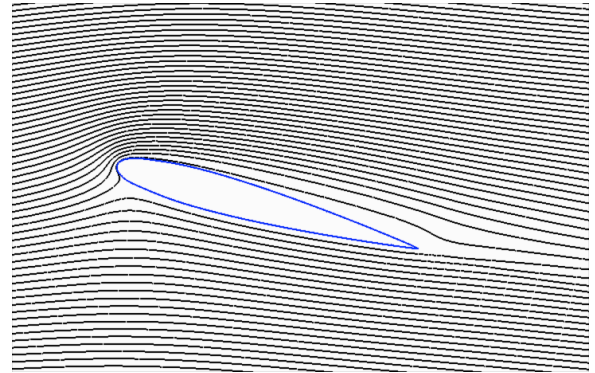
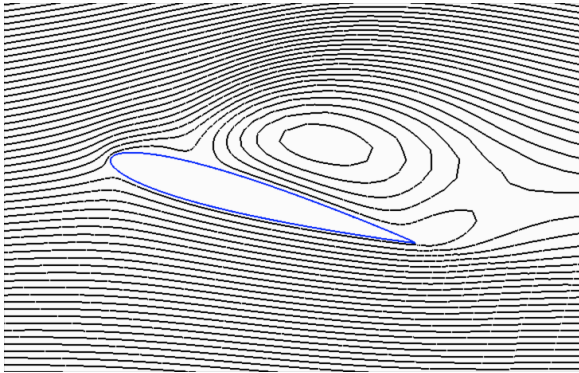


**Figure.4.e.1:** Streamlines, vorticity contours and surface pressure coefficient over the NACA0012 airfoil at  $\alpha=15.31^\circ$ .

**Figure.4.e.2:** Streamlines, vorticity contours and surface pressure coefficient over the DDLE airfoil at  $\alpha=15.31^\circ$ .

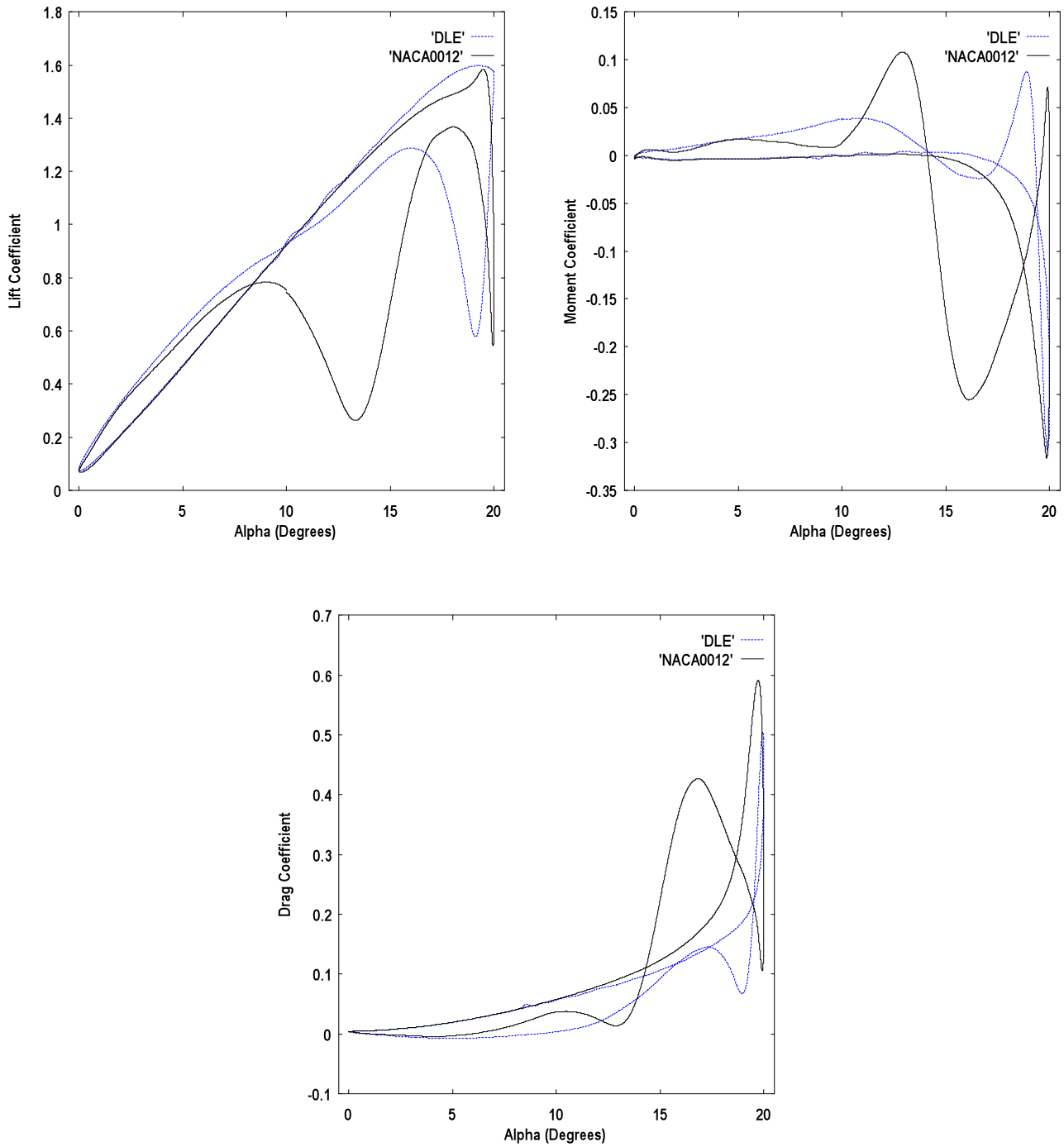


**Figure 5.** Lift, Drag and Pitching Moment Hysteresis Loops for the NACA 0012 and the DDLE Airfoils.

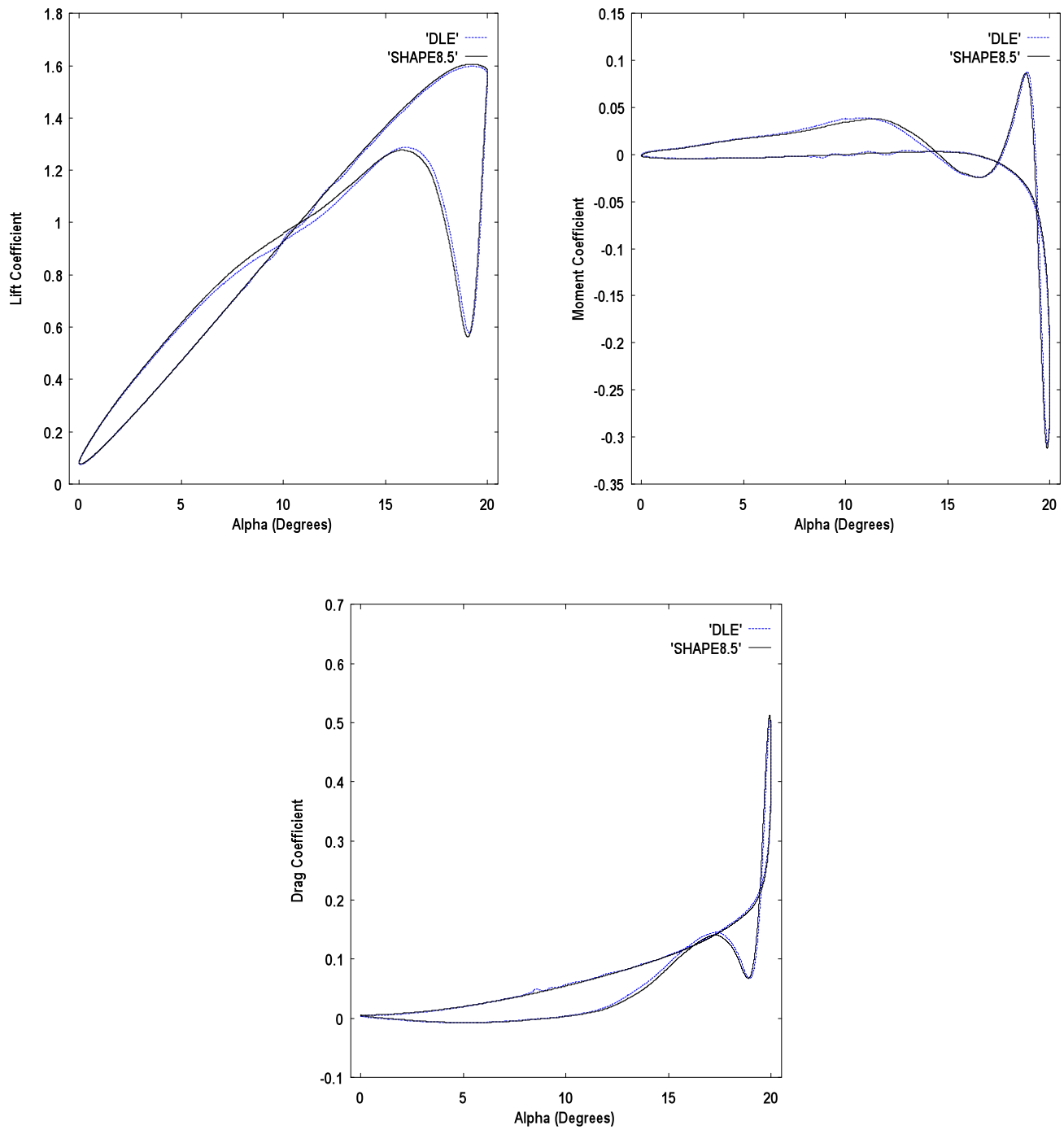


**Figure 6.** Comparison of the Load Hysteresis Characteristics between the DDLE Airfoil and the Fixed 8.5 Shape.

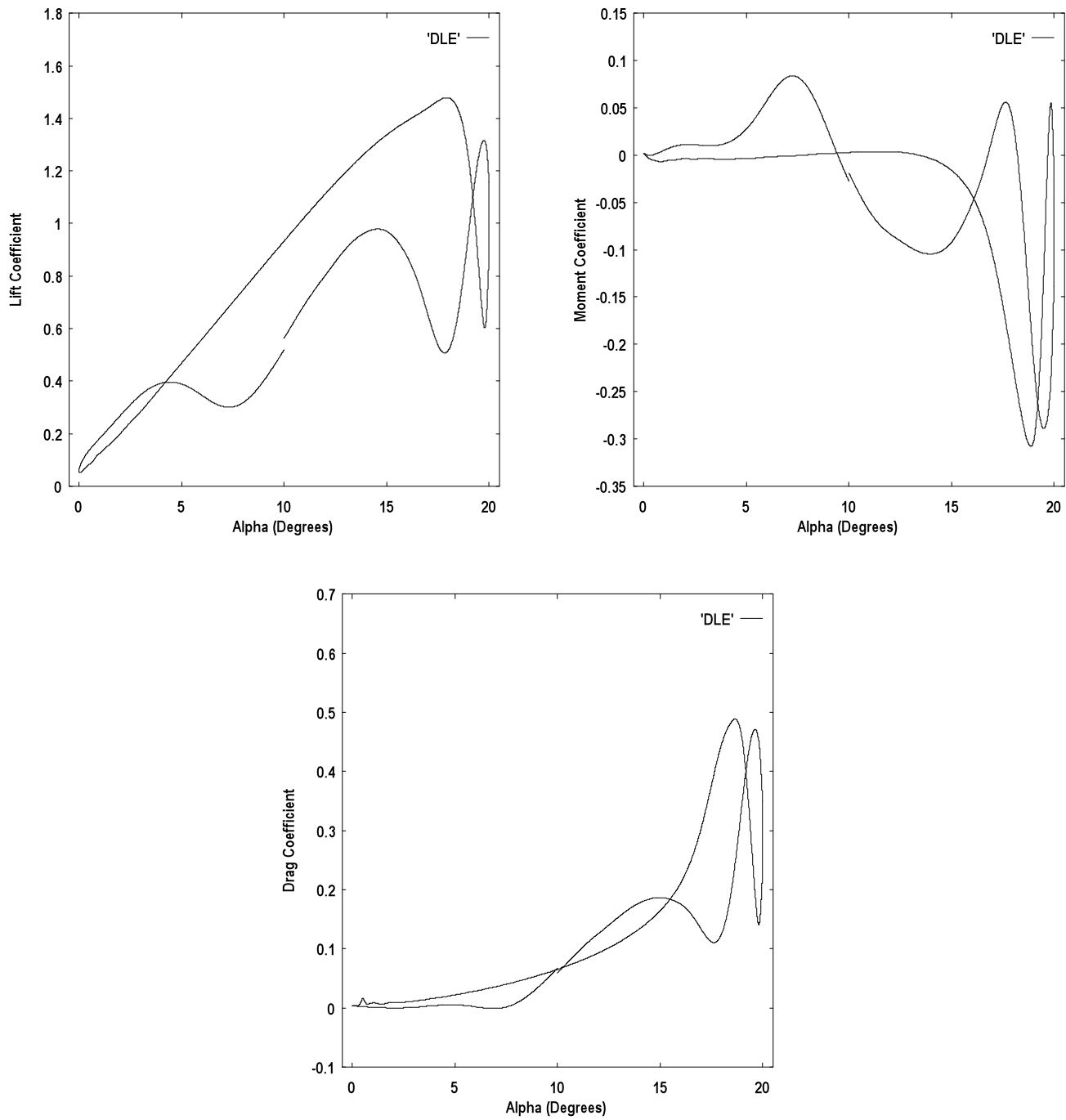


**Figure 7.** Dynamic Stall Load Hysterisis Characteristics of the DDLE Airfoil at M=0.4.